Integrated experimental and response surface methodology approach for metronidazole removal from hospital effluents by cellulose – iron oxide nanocomposite

Noor Zaman[1*], Farah Naz[2], Abdul Qadeer[1] , Khan Muhammad[2], Arshad Iqbal[3], Abul Sami[4], Sanam Rahojo[1], Masroor Abro[2]

[1] National Center of Excellence for Analytical Chemistry University of Sindh, Jamshoro, Pakistan
[2] Chemical Engineering Department Mehran University of Engineering and Technology, Jamshoro, Pakistan
[3] Chemical Engineering Department Dawood University of Engineering and Technology Karachi, Pakistan
[4] Chemical Engineering Department Qaid-e-Awam University of Engineering and Technology Nawabshah, Pakistan
* Corresponding author's e-mail: noorzamanshar@yahoo.com

ABSTRACT

Antibiotics are recognized as emerging environmental contaminants due to their persistence and adverse ecological impacts. Metronidazole (MMZ), a widely used nitroimidazole antibiotic, is of particular concern because of its extensive use and resistance to biodegradation. Its accumulation in the environment highlights the urgent need for effective removal strategies. The aim of current study was to synthesize economical cellulose-iron oxide nanocomposite (CI-NC) catalyst from an indigenous sugar mill waste bagasse as source for cellulose via co-precipitation process for the sequestration of MMZ antibiotics from hospital waste water. CI-NC was characterized by energy-dispersive X-ray EDX, scanning electron microscopy (SEM), UV-visible spectroscopy and Fourier transform spectroscopy (FTIR). The hospitals wastewater was analyzed using HPLC for presence of MMZ. Experiments were designed by faced centered central composite design (FCCCD) in deign expert 13 and response surface modeling (RSM) was employed for optimization of experimental variables used to analyze the main and interaction effects. The design variables were nanocomposite dose, pH, MNZ, temperature, hydrogen peroxide, and contact time. It was raveled that 98.00% degradation achieved at composite dose of 10 mg and MMZ 30 ppm, pH of 6, time of 30 min, temperature of 313 K, H_2O_2 and 0.6 mmol/L. A high degree of fit was achieved with the cubic model. The kinetic study revealed that the experimental data were best described by the pseudo-second-order kinetic model, with R^2 of 0.99. The present findings demonstrate the potential of CI-NC as sustainable and efficient material for the sequestration of MMZ antibiotics form hospital waste and pharmaceutical industries.

Keywords: metronidazole, response surface methodology, nanocomposite, water and water treatment, antibiotics.

INTRODUCTION

Antibiotics are newly identified pollutants that are used to cure and prevent infections in humans as well as animals (Zaidi et al 2025; Eapen, 2024; Eskandari et al., 2023). The thirty to ninety percent of antibiotics do not digest in bodies of humans or animals and are discharged into the environment via stool and urine (Guo et al., 2021; Wang et al., 2021). Antibiotics are a class of contaminants. They enter into the environment through the hospital effluent wastewater and the

excretion of drug metabolites due to inadequate metabolism (Guo et al., 2021). The metronidazole (MMZ) antibiotic belongs to the class of nitroimidazole, which is used to treat amoebiasis, trichomoniasis, and giardiasis diseases (Carrales-Alvarado et al., 2020; Ighalo et al., 2020). MMZ are usually released untreated in water bodies like in drinking water sources, wastewaters, and surface waters (Davarnejad et al., 2022; Santana et al., 2017). Since MMZ is non-biodegradable as well as carcinogenic, it has detrimental effects on both people as well as environment; thus, its

effective removal techniques must be developed. These techniques must be technological, environmental, and economical (Grenni et al., 2018). The natural polymer cellulose suitable for the breakdown of MMZ is found abundantly in sugarcane bagasse (SCB), about 32–45% (Al-Hazmi et al., 2024; Kumar et al., 2021; Olatunji, 2016; Rehm, 2010). The extracted cellulose (EC) is reactive, non-toxic, readily available, eco-friendly, biocompatible, biodegradable and can be readily modified by incorporating metal nanoparticles to synthesis a suitable catalyst (Al-Hazmi et al., 2024; Wang et al., 2016). The cellulose based nanocomposite materials easily integrate with metals to provide well-developed surface area for functionalized the degradation reaction (Fiszka Borzyszkowska et al., 2022). Carbon nanotubes (CNT), aluminum oxide (Al_2O_3), titanium oxide (TiO_2) and Iron Oxide (Fe_3O_4) nanoparticle (IONPs) can easily be integrated in cellulose to generate a suitable catalyst. The cellulose based -Fe_3O_4 nanocomposite has been widely used, as it is preferred for degradation of MMZ antibiotic drugs (Yadav et al., 2015). Because IONP is inexpensive, it can be easily oxidized to generate free radicals, as well as quickly separated by an external magnet (Rajabi and Nasiri, 2021). Antibiotics have been effectively extracted from aqueous solutions using oxidation techniques like photo-Fenton reactions. Common disinfection methods, including ozonation (O_3), ultraviolet light (UV), and chlorination raise the potential for the production of carcinogenic disinfection by-products (DBP), but highly resistant waterborne bacteria are less amenable to these methods (Gahrouei et al. 2024; Zhang et al. (2024). Moving bed biofilm reactor (MBBR) removes 27.4% in 24-hour retention period, the polypyrrole was removed via adsorption, which is capable of removing 38.9% of MMZ. The processes above produce secondary pollutants as well as consume high levels of energy and chemicals (Eskandari et al., 2023). Compared to other approaches, photo-Fenton-processes are efficient, economical as well as time-efficient (Asgari et al., 2019). The photo-Fenton process does not produce secondary pollutants by using heterogeneous catalysts (Mansoori et al., 2021; Wang et al., 2020). IONPs are heterogeneous catalysts responsible for generation of hydroxyl radicals to initiate the photo-Fenton process (Pastrana-Martínez et al., 2015). IONPs increase the surface area of the composite and increase the number

of reacting sites, which accelerates the reaction (Wang et al., 2018). The breakdown of hydrocarbon is aided by auxiliary catalyst to the photo Fenton process, which increases the oxidation and reduction cycle by generating the hydroxyl radicals (Sun et al., 2019). One practical statistical technique that may be used to plan the experiment and examine the variables is response surface methodology (RSM) (Davarnejad et al., 2022). The detailed analysis of literature revealed there is no concrete study available on utilization of indigenous source biomass in cellulose-iron oxide nanocomposite (CI-NC) synthesis and its utilization for local hospital waste. At the same time, RSM analysis of experimental results has not been conducted.

This study aimed to synthesize CI-NC, an economical and green nanocomposite using locally available bagasse biomass, and to evaluate its efficiency for the removal of carcinogenic antibiotic MMZ from hospital wastewater. For the further investigation into removal mechanism, the kinetic modeling was performed. For this purpose, the composite was synthesized, characterized using physical and chemical analyses, and its degradation performance was optimized *via* RSM using Design Expert 13.0. The significant contribution of this work emerges from the use of locally available sugarcane bagasse as a renewable, low-cost, and abundant resource. Moreover, CI-NC exhibits multifunctionality, combining adsorption, photocatalytic degradation, and magnetic separability making it a sustainable, cost-effective, and easily retrievable solution for treating persistent pharmaceutical pollutants in wastewater, particularly in resource-limited treatment options.

MATERIAL AND CHEMICALS

Reagents

All chemicals used in this study, including ferric chloride hexahydrate (FeCl₃•6H2O) 99%, ferrous chloride tetrahydrate (FeCl₂•4H₂O) 99.9%, ammonium hydroxide (NH₄OH) 99.9%, sodium hydroxide (NaOH) 80%, urea (CH₄N₂O) 99.5%, and hydrogen peroxide (H₂O₂) 35% were of analytical grade. These were purchased from Sigma Aldrich Chemicals. Sterilized distilled water with a conductivity of 1 μS/cm, obtained from laboratory distilled water plant was used in experiments. The Matiari Sugar Mills Limited,

Matiari Sindh, provided the Sugar cane bagasse. Deionized and double-distilled water purchased from Al-baruni scientific store in Hyderabad was used to prepare all the solutions required in experiments.

Sample collection, preservation and analysis

Hospital wastewater samples were collected from Liaquat University of Medical and Health Sciences Jamshoro, during peak operational hours in pre-cleaned, high-density polyethylene containers. The containers were immediately sealed, labeled, and transported to the laboratory under cooled conditions (4 °C) to prevent microbial degradation. The sample analysis was performed using a high pressure liquid chromatography (HPLC) model C-300.

Preparation of iron oxide nanoparticle

IONPs was synthesized by employing the method used by Mehta et al. (1997). The Fe^{2+} and Fe^{3+} were precipitated by ammonium hydroxide (NH_4OH) and treated hydrothermally at molar ratio of 2:1, the ferric and ferrous chlorides were dissolved in 0.3 M water. The addition of NH_4OH 15.6 M at 25 °C with vigorous stirring produced chemical precipitation. In the course of the reaction, the pH was kept at roughly 10. After heating at 80 °C for 30 minutes, the precipitates were repeatedly washed with ethanol and water followed by dehydration at 70 °C in furnace to obtain IONPs.

Extraction of cellulose from sugar cane bagasse

Sugarcane bagasse (SCB) was sourced from a local sugar production facility from Matiari Sugar Mills Limited, Matiari Sindh. The collected bagasse was manually stripped and sun-dried for three days. After drying, the material was crushed into smaller fragments and further dried in an oven at 100 °C for twenty-four hours. The dried bagasse was then ground into a fine powder using an electric grinder, washed thoroughly with double-distilled deionized water, and oven-dried again for twenty-four hours. For the bleaching process, the powdered bagasse was treated with 0.12 M hydrogen peroxide (H_2O_2) solution at a fiber-to-liquid ratio of 1:70, with the pH adjusted to 4 using a few drops of 8 M

acetic acid (CH_3COOH). The mixture was boiled for five hours to remove lignin. After boiling, the suspension was centrifuged and repeatedly washed with double-distilled deionized water until a neutral pH 7 was achieved. Subsequently, the residue was boiled in 0.4 M sodium sulfite (Na_2SO_3) solution for 5 hours and rinsed thoroughly with deionized water to ensure the complete removal of lignin and partial elimination of hemicellulose. The treated residue was then subjected to further boiling in 4.0 M sodium hydroxide (NaOH) solution for five hours to eliminate the remaining hemicellulose content. The resulting cellulose was filtered, centrifuged, and washed with double-distilled deionized water. To enhance purity, the cellulose was dispersed in 50 mL of 0.7 M dimethyl sulfoxide (DMSO) and maintained in a water bath at 80 °C for three hours. Following this treatment, the sample was centrifuged, washed extensively with double-distilled deionized water, then it was dried. The final EC was stored in an airtight container for degradation of MMZ.

Synthesis of cellulose-iron oxide nanocomposite

Cellulose-iron oxide nanocomposite synthesized by 0.2 grams of IONPs was suspended inside 20 milliliters of EC. Obtained solution was agitated at 35 °C +/- 2°C for two hours at 130 rpm. The detailed schematic diagram of synthesized resultant solution of CI-NC material shown in Figure 1.

Characterization of CI-NC

The prepared materials were characterized by various analytical techniques, including UV-visible spectrophotometry, Fourier transform infrared (FTIR) was performed to recognize the presence of association of functional group attachment, XRD analysis was used to confirm the presence of crystalline structure of iron oxide characteristics in synthesized IONPs and to prove the existence of amorphous and semi crystalline lignocellulose presence of bagasse in CI-NC material. UV-visible spectrophotometry and SEM was conducted to observe the morphology used for verifying the EC and CI-NC material (DineshKumar and Purushothaman, 2016). The energy dispersive X-ray EDX was used to
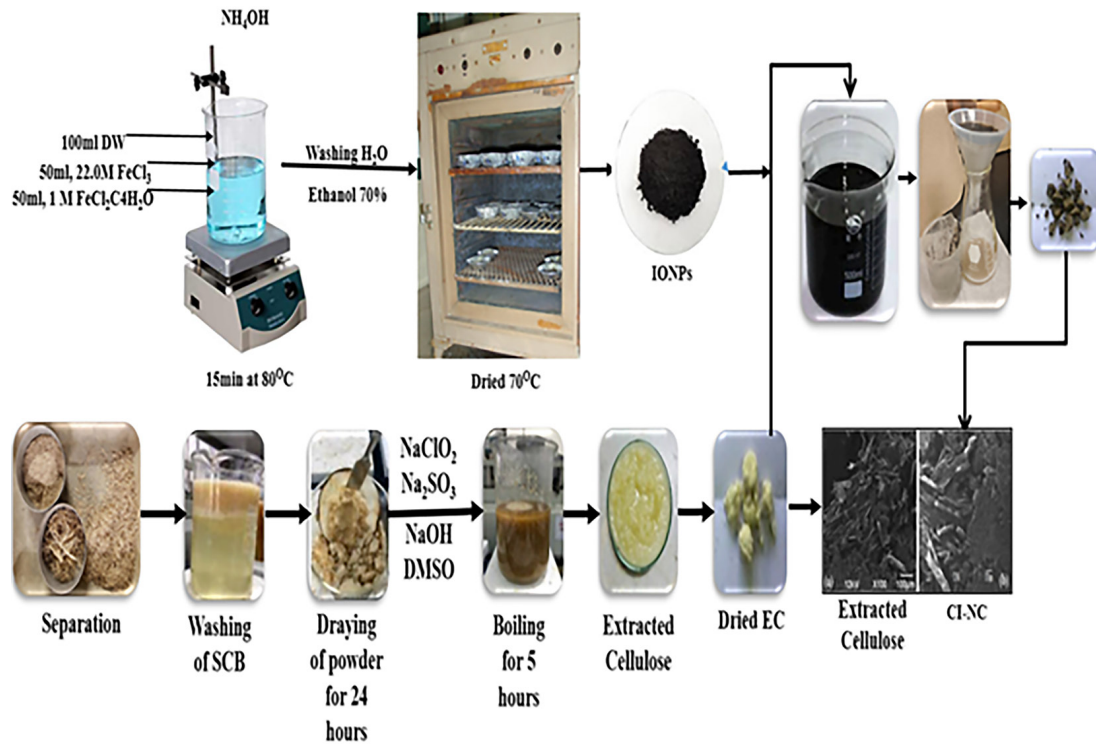
Figure 1. Schematic diagram of synthesis scheme of CI-NC

identify and quantify the elemental composition of CI-NC (Lalegül-Ülker and Elçin, 2021).

Experimental design response surface methodology

In the current study, RSM was used to examine the interconnection results of six independent variables including A: pH, B: dose of composite, C: drug conc. D: temperature, E: time, F: H_2O_2, on Y: by CI-NC degradation of MMZ drug. Faced Centered Central composite design (FCCCD), was applied to create a three-level, six -factor design (Bala et al., 2017). The low, middle, and high levels of the design factors were denoted by the standard codes -1, 0, and 1, respectively. The table gives the precise values for every degree of every design factor (Table 1).

The analysis of the response was conducted in Design Expert 13 using a regression equation. The primary effects of the independent variables, or design factors, are labeled A, B, C, D, E, F whereas AB, AC, AD, AE, AF, BC, BD, BE, BF, CD, CE, CF, DE, DF, and EF stand for the interaction effects of these components.

Following each run, the UV-vis spectrophotometer used the following equation to analyze

the beginning and final concentrations of MMZ effluent at a maximum wavelength of 320 nm.

$$Removal\% = \frac{C_o - C_t}{C_o} \times 100 \qquad (1)$$

where: C_o and C_t denote the initial and equilibrium concentrations of MMZ respectively.

RESULTS AND DISCUSSION

The results of synthesized material CI-NC through UV, XRF, FTIR and SEM is presented below. Removal of MMZ from hospital wastewater is also presented along with the analysis of experimental results data using RSM is given.

Characterization of cellulose iron oxide nanocomposite

UV analysis

Synthesized IONPs were sonicated for 30 minutes in deionized water to provide a transparent colloid solution for UV examination.

The absorbance spectrum in Figure 2 (a) showed IONPs peak at 286 nm, in Figure 2 (b) absorption peak at 280 nm and 307 nm for EC, while the values of EC polymer values decreases

Table 1. Level of parameters for Faced Centered Central Composite Design (FCCCD)

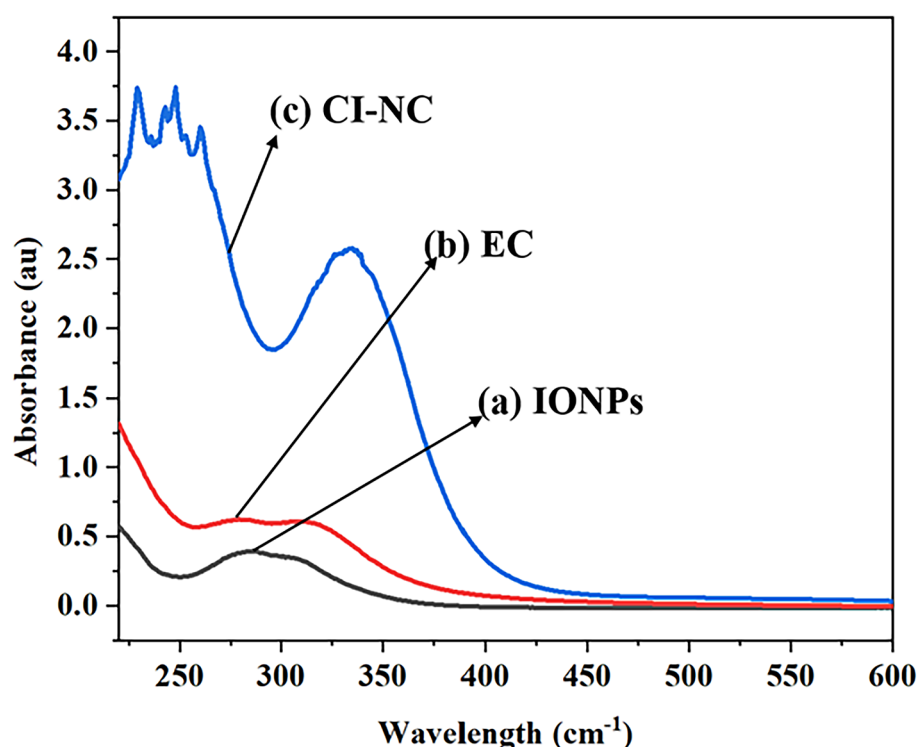| Variables	Symbol	Levels		
		Low level (-1)	Intermediate level (0)	Higher level (1)
pH	A	2	6	10
Dose of composite (mg)	B	5	10	15
Drug conc. (mg/L)	C	30	40	50
Temperature (K)	D	313	318	323
Time (min)	E	10	20	30
H_2O_2 (mM)	F	0.2	0.7	1.2

Figure 2. UV-Visible analysis of a: IONPs, b: EC c: CI-NC

from 280 nm to 248, while other increases from 307 to 332 nm, which proves complete entering of IONPs inside pores of EC polymer material in Figure 2 (c) (Mun et al. 2015)

Fourier Transform Infrared Spectroscopy (FTIR)

Fourier Transform Infrared Spectroscopy (FTIR) was employed to identify the functional groups and chemical bonds in material by measuring its infrared absorption spectrum.

Figure 3 illustrates the FTIR spectrum of (a) IONPs, (b) EC (c) CI-NC. The overall % of absorbance transmitted for CI-NC was higher than EC due to the interaction that occurred between CI-NC

and the OH groups. The bands at 1628 cm^{-1}: Short band that indicates H-O-H bending of absorbed water, 577–631 cm^{-1} indicate the presence of iron-oxygen (Fe-O) in IONPs. The carbonyl group of EC and some hemicelluloses are linked to the band 3381 cm^{-1}, which is associated with OH stretching, and the 2917 cm^{-1} CH stretching and deformation vibration at 1740 cm^{-1}. CH$_2$ bending, CH bending, OH bending, and CH$_2$ rocking vibration are the respective causes of the band at about 1443 cm^{-1}, indicating the EC. The tensile vibrations of the O-H and C-H groups, the flexural and modified vibrations of the C-H group, and the flexural vibrations for the CI-NC were linked to the absorption bands that were evident at wavelengths of 2917, 3432, 1444, and 1049 cm^{-1}. The peak at wavelength of
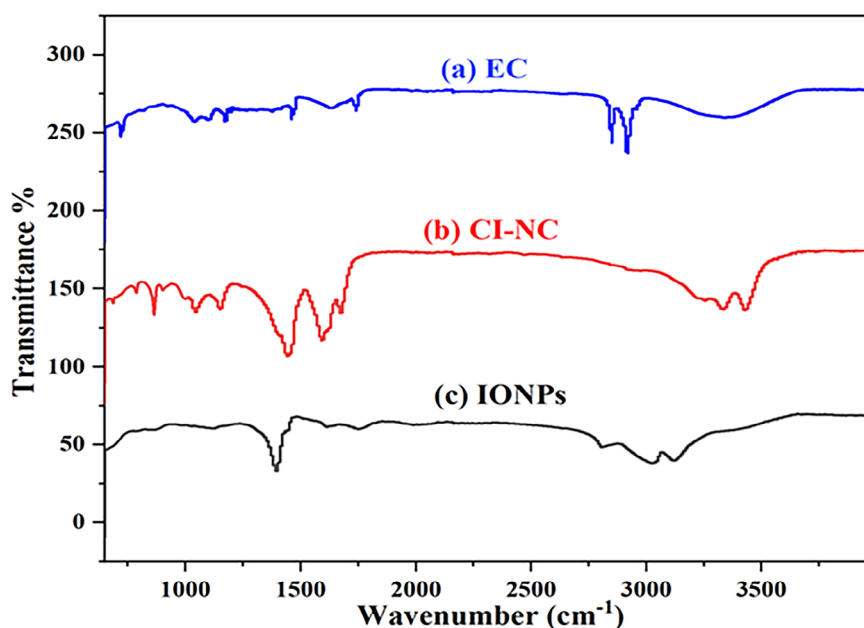
Figure 3. FTIR Spectroscopic analysis of a: EC, b: CI-NC, c: IONPs

582 cm^{-1} shows the IONPs in EC polymer. The development of the interaction between the O-H and the Fe_3O_4 group is responsible for the broadness of the absorption bands of hydroxyl group and its migration to the lower wavelength in the synthesized CI-NC (Azizi, 2020).

Scanning electron microscopy (SEM)

SEM is a powerful imaging technique used to analyze the surface morphology, particle size, and structural properties of materials at a high resolution.

Figure 4 illustrates the SEM analysis of EC and CI-NC. In Figure 4 (a), EC exhibits a semi-spherical shape, with notably uniform and narrow size distribution. The semi-spherical shape maximizes light capture and increases charge carriers under the visible or ultraviolet light, thereby promoting the effective degradation of organic material. IONPs were found to accumulate on the surface and within EC. Additionally, the large flake-like shape was seen, indicating the local agglomeration and accumulation consistent with the findings of (Azizi, 2020). Contrastingly, the SEM image of CI-NC in Figure 4b demonstrates a porous structure with several voids, decreased particle agglomeration, and improved dispersion of IONPs throughout the nanocomposite
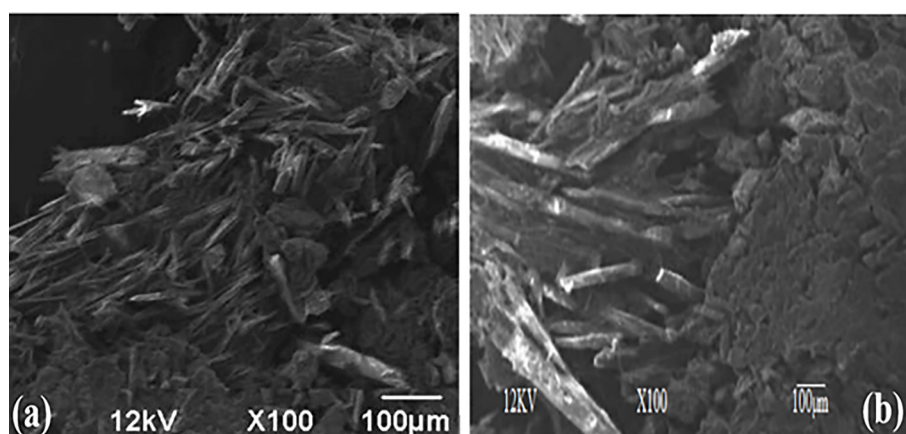

Figure 4. SEM of a: EC and b: CI-NC

Energy dispersive X-ray spectroscopy (EDX)

EDX was performed to confirm the presence of carbon, nitrogen, sulfur, sodium and other elements in MMZ specimen.

In Figure 5, the EDX spectrum of (a) EC (b) CI-NC demonstrated the compositional changes resulted by impregnation of EC with iron oxide. EDX images present the C, O and Fe on the of CI-NC confirmed the iron nanoparticle had formed on the layer of EC (Xiong et al., 2014). EDX result also evidenced that EC contains 100% of carbon while in CI-NC presence of carbon 13.78%, oxygen 47.66% and iron 38.55%.

Investigation of critical experimental parameters

A comprehensive parametric investigation was conducted to analyze the factors influencing the degradation of the MMZ antibiotic using a CI-NC. The removal efficiency was investigated under varying experimental conditions, including pH (2-6), nanocomposite dosage (5–15 mg/L), initial drug concentration (20–50 mg/L), temperature (313–323 K), reaction time (10–30 min), and H_2O_2 concentration (0.2–1.2 mg/L). Experimental results revealed that a maximum degradation efficiency of 97.87% was achieved under optimal conditions; pH 6, nanocomposite dose 10 mg/L, initial drug concentration 20 mg/L, temperature 313, reaction time 20 min, and H_2O_2 concentration 0.7 mg/L. A similar trend was reported by (Davarnejad et al., 2022), which is consistent with the expected enhancement in degradation efficiency due to the incorporation IONPs into the

cellulose matrix. This results into increased availability of active binding sites, thereby facilitating an enhanced degradation performance (Wang et al., 2018).

Adsorption study of metronidazole (MMZ) in CI-NC

The adsorption behavior of MMZ onto the synthesized cellulose-based iron oxide nanocomposite was systematically investigated. Batch experiments were conducted to evaluate the effects of key parameters, such as pH, drug concentration, time, dose of composite and H_2O_2 concentration.

RSM results

To optimize the adsorption conditions and model the interaction effects, response surface methodology (RSM) was used providing insight into the significance and interaction of variables towards adsorption efficiency. Table 2 presents the experimental design and response values.

ANOVA and regression model results

To develop the regression model and determine the best-fitting equation, an analysis was conducted to predict degradation of MMZ. The influencing elements that were taken into consideration were A, B, C, D, and E. Table 3 summarizes the interaction effects of these components as follows: AB, AC, AD, AE, AF, BC, BD, BE, BF, CD, CE, CF, DE, DF, and EF. The resulting equation illustrates the main and interaction effects of all design variables, where a positive sign indicates a synergistic effect, enhancing the response,
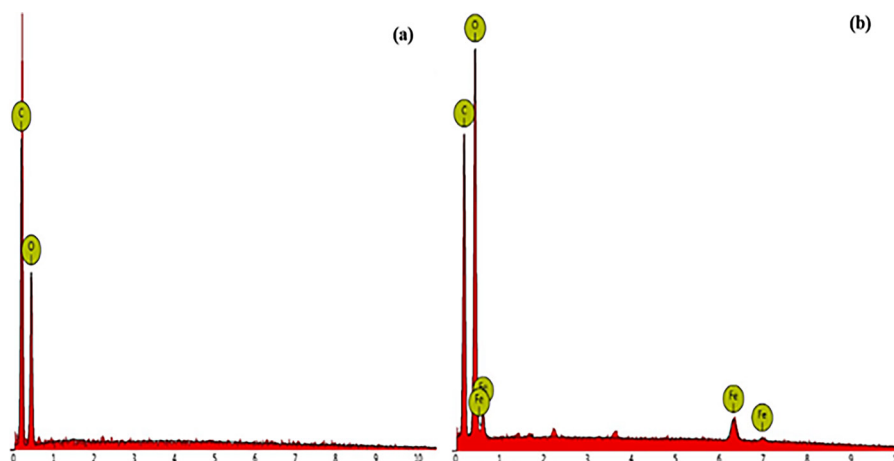

Figure 5. EDX Analyses of (a) EC (b) CI-NC

Table 2. Experimental design for degradation of MMZ

Run	A: pH	B: Dose of composite (g)	C: Drug Conc. (mg/l)	D: Temperature (K)	E: Time (min)	F: H_2O_2 (mM)	MMZ degradation (Exp)
1	6	10	40	318	20	0.2	81
2	6	10	40	323	20	0.7	60
3	10	15	30	323	10	1.2	32
4	6	10	40	318	20	0.7	98
5	2	5	30	323	30	0.2	10
6	2	15	50	313	10	0.2	10
7	2	10	40	318	20	0.7	93
8	10	15	30	313	30	1.2	35
9	2	15	30	313	10	1.2	28
10	2	15	30	323	30	1.2	20
11	6	10	40	318	20	0.7	98
12	2	15	50	323	30	0.2	24
13	6	10	40	318	10	0.7	69
14	10	5	50	323	10	1.2	20
15	2	5	50	313	10	1.2	15
16	2	5	30	313	10	0.2	27
17	6	10	40	318	20	0.7	87
18	2	5	50	323	30	1.2	35
19	10	5	30	323	10	0.2	20
20	10	10	40	318	20	0.7	53
21	6	5	40	318	20	0.7	60
22	10	5	50	313	30	1.2	32
23	10	5	30	313	30	0.2	18
24	6	10	40	318	30	0.7	89
25	6	10	40	318	20	0.7	98
26	10	15	50	323	10	0.2	32
27	6	10	30	318	20	0.7	88
28	6	10	50	318	20	0.7	75
29	6	10	40	313	20	0.7	98
30	10	15	50	313	30	0.2	35
31	6	10	40	318	20	0.7	98
32	6	15	40	318	20	0.7	90
33	6	10	40	318	20	1.2	94

while a negative sign represents an antagonistic effect, reducing the response. A detailed examination for these effects was carried out to assess their impact on the model parameters.

The F-value of 50.01 for the model suggests that the model is important. The likelihood that an F-value this large may be caused by noise is only 0.08%. Model terms are considered significant when the P-value is less than 0.0500. A, B, D, E, AE, CE, CF, DE, A², B², C², D², and E² are important model terms in this instance (Eskandari et al., 2023).

In Table 4, the high coefficient of determination R² 0.99 and the adjusted R² 0.97 for MMZ degradation demonstrate a reasonable correlation between experimental and predicted results(Mosavi et al., 2021).

Response contour plots

Figure 6 represents the contour plots illustrating the interaction effects of six variables on MMZ degradation (%) from RSM analysis. Each plot depicts the combined influence of two factors while keeping the others constant, revealing how different parameter combinations affect degradation efficiency. The color gradient

Table 3. ANOVA for cubic model (Response: MMZ degradation (%)

Source	Sum of squire	Df	Mean Squire	F-Value	P-Value	
Model	33886.72	28	1210.24	50.01	0.0008	Significant
A-pH	800.00	1	800.00	33.06	0.0045	
B-Dose of composite	450.00	1	450.00	18.60	0.0125	
C-Drug Conc	84.50	1	84.50	3.49	0.1350	
D-Temperature	722.00	1	722.00	29.83	0.0055	
E-Time	200.00	1	200.00	8.26	0.0452	
F-H2O2	84.50	1	84.50	3.49	0.1350	
AB	150.06	1	150.06	6.20	0.0675	
AC	14.06	1	14.06	0.5811	0.4884	
AD	126.56	1	126.56	5.23	0.0841	
AE	612.56	1	612.56	25.31	0.0073	
AF	10.56	1	10.56	0.4365	0.5449	
BC	27.56	1	27.56	1.14	0.3460	
BD	3.06	1	3.06	0.1265	0.7400	
BE	0.0625	1	0.0625	0.0026	0.9619	
BF	95.06	1	95.06	3.93	0.1185	
CD	126.56	1	126.56	5.23	0.0841	
CE	333.06	1	333.06	13.76	0.0207	
CF	280.56	1	280.56	11.59	0.0272	
DE	976.56	1	976.56	40.35	0.0031	
DF	0.0625	1	0.0625	0.0026	0.9619	
EF	52.56	1	52.56	2.17	0.2145	
A^2	742.63	1	742.63	30.69	0.0052	
B^2	618.06	1	618.06	25.54	0.0072	
C^2	292.13	1	292.13	12.07	0.0255	
D^2	403.20	1	403.20	16.66	0.0151	
E^2	403.20	1	403.20	16.66	0.0151	
F^2	98.41	1	98.41	4.07	0.1139	

Table 4. Regression model equation for response against the different factors and their interaction

Regression model equation	R^2	Adjusted R^2
MMZ degradation (%)= +95.80-20.00 A+15.00 B-6.50 C19.00D+10.00 E+6.50 F+3.06 AB+0.9375 AC+8.44 AD-18.56 AE-0.8125 AF+3.94 BC+0.4375 BD-0.0625 BE-7.31 BF+2.81 CD+4.56 CE-23.44 DE+0.0625 DF+1.81 EF-22.80 A^2-20.80 B^2-14.30 C^2-16.80 D^2-16.80 E^2-8.30 F^2	0.9972	0.9772

from blue to red indicates increasing degradation levels, with red representing the highest efficiency. Contour lines labeled with percentages (e.g., 0, 20, 40, 60, 80) mark specific degradation levels, showing how sensitive MMZ degradation is to changes in the interacting parameters. The individual plots reveal critical insights into the degradation process. For higher composite doses and lower pH values generally enhance degradation efficiency. This increased trend could be the result of more active sites, which raises the amount of MMZ adsorption on the CI-NC surface. Furthermore, increasing the quantity of active sites can boost the generation of reactive species •OH and improve light adsorption (Bashiri et al., 2020). Increasing drug concentration tends to reduce efficiency, while temperature variations have a moderate influence. The interaction between pH and H_2O_2
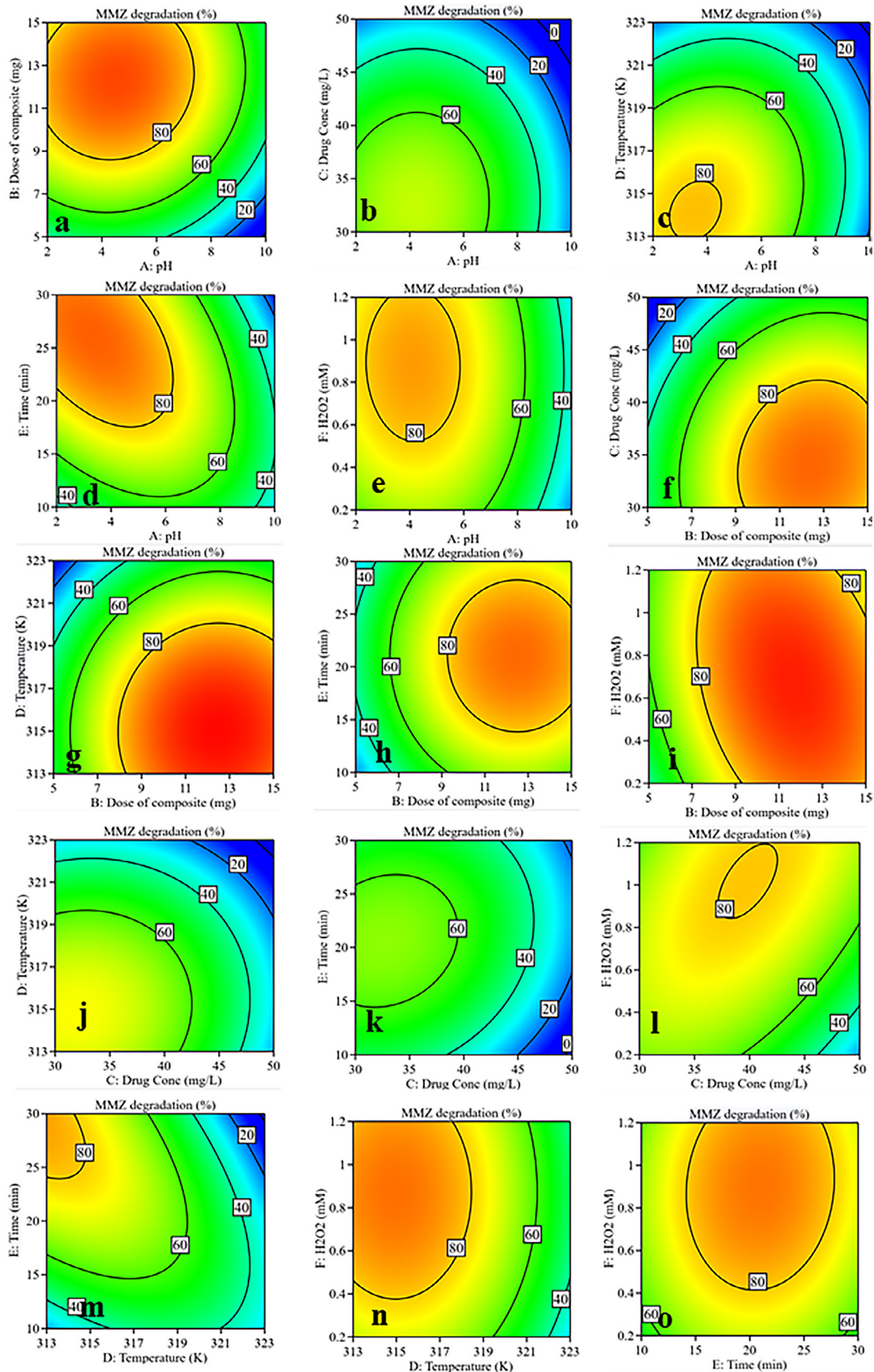
Figure 6. Contour plots of a: dose of composite and pH, b: drug Conc: and pH, c: temperature and pH, d: time and pH, e: H_2O_2 and pH, f: drug conc: and dose of composite, g: temperature and dose of composite, h: time and dose of composite, i: H_2O_2 and dose of composite, j: temperature drug conc, k: time and drug conc:, l: H_2O_2 and drug conc:, m: time and temperature, n: H_2O_2 and temperature, o: H_2O_2 and time shows interaction effects of CI-NC on MMZ degradation
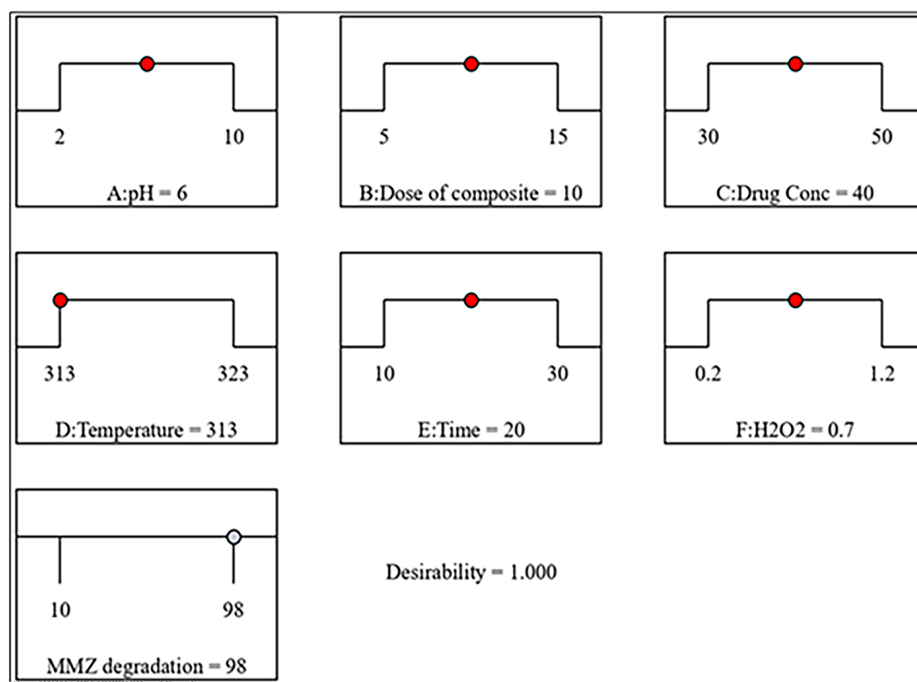
Figure 7. Optimization ramp

concentration suggested that higher oxidant levels improve degradation.

Optimization of parameter

Figure 7 illustrates the optimization of parameters by RSM for MMZ degradation.

It was revealed from the above optimization ramp that six independent variables show the maximum degradation of MMZ at: pH (6), dose of composite (10 mg/L), drug concentration (40 mg/L), temperature (313 K), time (20 minutes), and H_2O_2 concentration (0.7 mg/L). The above optimization ramp indicates the optimal values for each parameter, suggesting that these conditions are ideal for achieving the maximum possible degradation of MMZ. The response variable MMZ was 98% degraded with above optimized variables values. Additionally, the desirability score of 1.000 confirms that these conditions yield the most favorable outcome, as a desirability value of 1 represents the best possible solution.

Prediction profiler

Figure 8 represents a prediction profiler from a statistical analysis, likely from response surface methodology (RSM). The profiler visually depicts how different independent variables influence the response variable, in term of MMZ degradation

(%). Each plot represents the effect of a single factor on MMZ degradation while keeping other factors constant (Betiku et al., 2021).

Performance evaluation by RSM

Figure 9 illustrates the performance of the model using a Predicted vs. Actual plot, which visually demonstrates the correlation between experimental and model-predicted values

The data points in this plot closely align with the diagonal line, indicating that the model has high accuracy and reliability in predicting MMZ degradation (Malika and Sonawane, 2021). The smooth color gradient suggests a well-fitted model without significant fluctuations or inconsistencies. Overall, this graph confirms that the model provides strong predictive performance for MMZ degradation.

Kinetic study of antibiotic degradation

The kinetics of MMZ degradation was assessed by using the pseudo-first-order and pseudo-second-order models. The obtained outcomes of rate constant for theoretical and calculated values do not come in match for first-order model where values of theoretical and calculated measured was 3.92 and -0.445662298 mg/g respectively. In the case of pseudo-second order
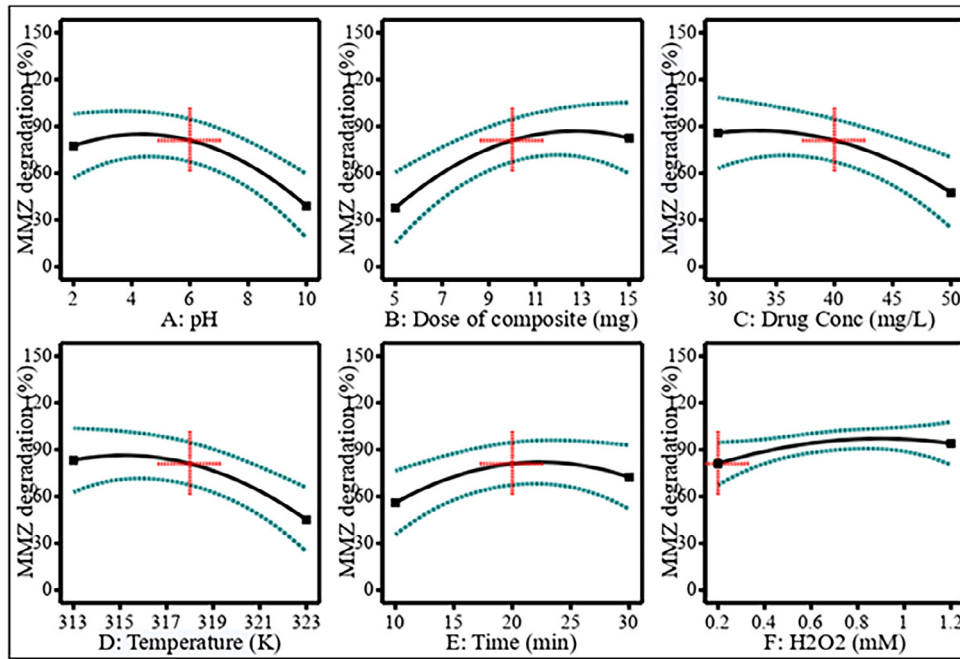
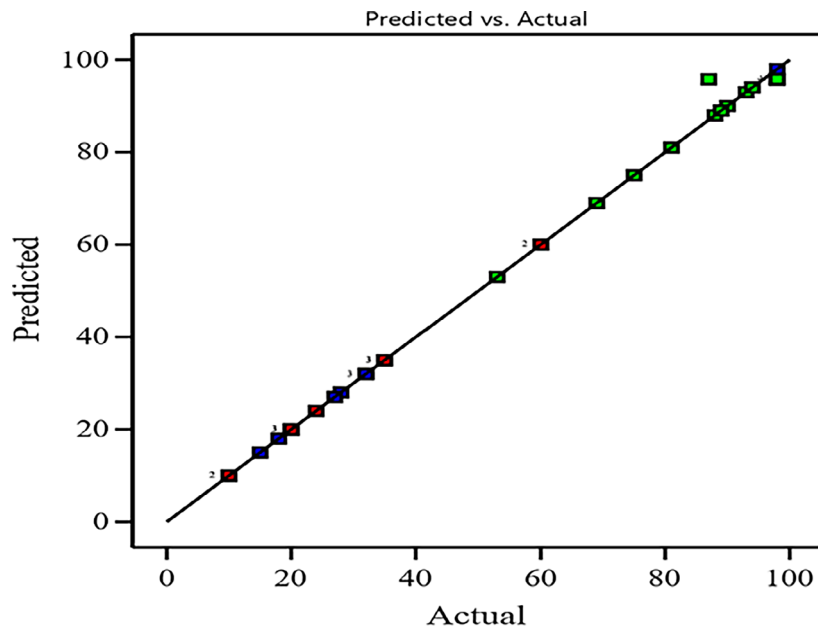**Figure 8.** Prediction profiler for MMZ degradation

Figure 9. Actual vs predicted value of MMZ degradation

model, the obtained results of rate constant for theoretical and calculated values are satisfied for second-order model where the measured values for theoretical and calculated was found as 3.93 and 4.12 mg/g, respectively. The obtained results confirm the experimental data with the pseudo-second-order kinetics model for MMZ degradation process for other researchers as well (Zhou et al., 2018). Fitting of pseudo second order kinetic model confirm the mechanism

of chemisorption for removal of MMZ from hospital waste. The adsorption capacity of synthesized SI-NC related to the availability of active sites rather than just the concentration of MMZ in solution. The model assumes that the adsorption rate is proportional to the square of the number of unoccupied sites, reflecting stronger and possibly irreversible interactions. It correlates high adsorption efficiency and selectivity, especially due to the presence of functional
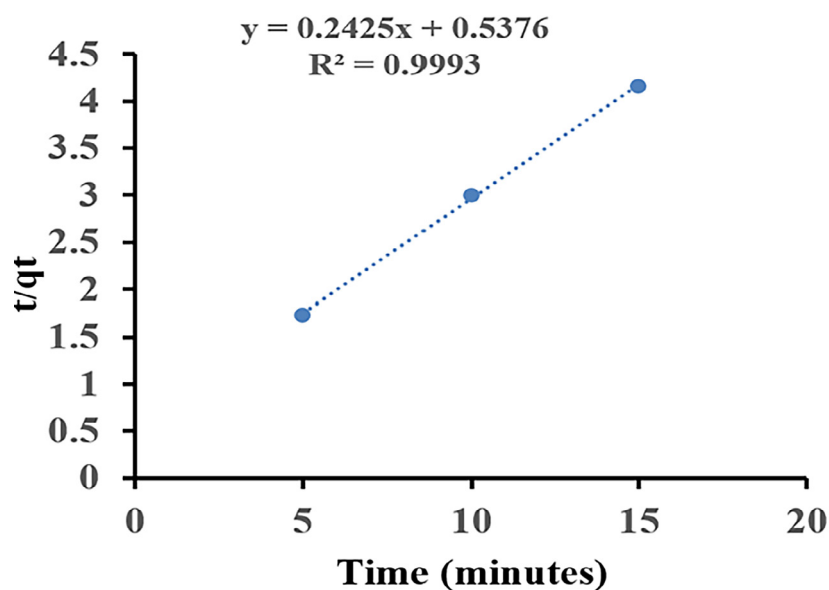
$$y = 0.2425x + 0.5376$$
$$R^2 = 0.9993$$

Figure 10. Pseudo-second-order model kinetics model of MMZ degradation
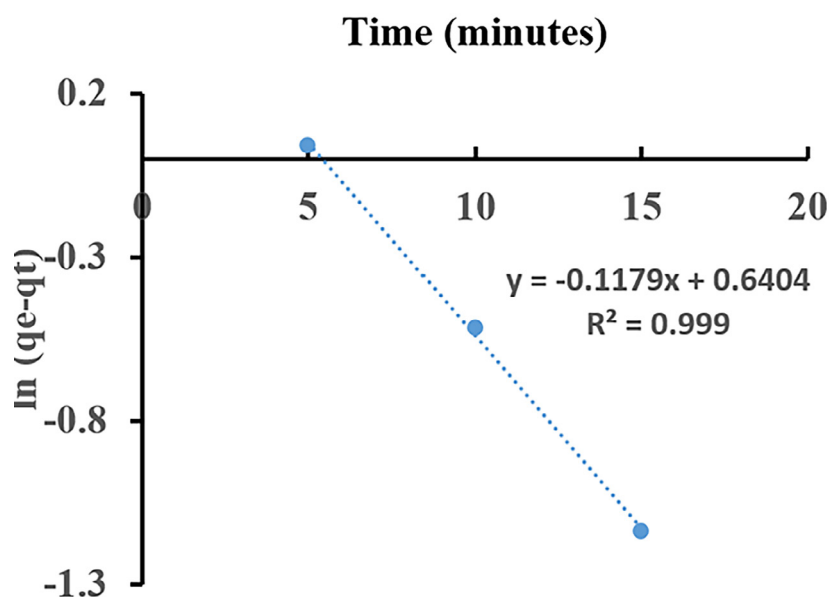
$$y = -0.1179x + 0.6404$$
$$R^2 = 0.999$$

Figure 11. Pseudo-first -order model kinetics model of MMZ degradation

Table 5. Comparison of current study with literature

Process	Optimal condition					Removal efficiency	Reference
	pH	$[MMZ]_0$ mg/L,	Catalyst dose (mg/L)	$[H_2O_2]_0$ (mmol/L)	Time Mint	%	
Fe_3O_4/Cellulose nanocomposite for metronidazole degradation	6	10	40	0.7	30	98	This study
Alginate-based hydrogel with bimetallic iron-copper composite	3.5	10		33.17	85	95	(Davarnejad et al., 2022)
Photo-Fenton process with magnetic Fe_3O_4@PBC composite	3	300	0.4	60	-	95	(Cai et al., 2020)
Heterogeneous Fenton process with modified alginate beads	10	10	50	-	-	94	(Titouhi and Belgaied, 2016)
Nano-ZnO/UV photocatalytic process	3	80	1500	-	180	96.55	(Farzadkia et al., 2014)

groups on cellulose or iron oxide in composite. First- and second-order kinetic models plots for antibiotics MMZ are listed in Figures 10 and 11.

The experimental findings were compared with the previously reported studies to validate the adsorption performance of the cellulose-based iron oxide nanocomposite (Table 5). Parameters such as pH, nanocomposite dose, initial drug concentration, temperature, reaction time, and H_2O_2 concentration against existing literature on similar adsorbents.

CONCLUSIONS

Alkaline pretreatment successfully removed the EC from SCB and the co-precipitation method of synthesizing IONPs and CI-NC was confirmed by FTIR flourier transform spectroscopy, UV-visible spectroscopy. X-ray dispersive diffraction (EDX) with SEM. The statistical analysis confirmed the accuracy of the predicted models of MMZ degradation. RSM results based on FCCCD showed that increasing CI-NC concentration and decreasing the pH concentration positively influence on the response. The increasing the pH and MMZ concentration have negative effect on degradation. Hydroxyl radicals, were found to be the reactive agents for the decomposition of MMZ. The rate constant studies showed the degradation of MMZ by CI-NC is second order reaction. The regression model's ability to predict the MMZ degradation was demonstrated by ANOVA. The catalyst CI-NC quantity of 40.0 mg/L, beginning pH of 6.0, MMZ concentration of 10 mg/L, H_2O_2 concentration of 0.6 mmol/L, temperature of 313 kelvin, and reaction time of 20 minutes were found to be the ideal conditions for 95.8% based on mode and 98.0% based on tests. Consequently, there was good agreement between the model's results and the experimental ones.

Acknowledgements

REFERENCES

1. Al-Hazmi, H. E., Łuczak, J., Habibzadeh, S., Hasanin, M. S., Mohammadi, A., Esmaeili, A.,… Badawi, M. (2024). Polysaccharide nanocomposites in wastewater treatment: A review. *Chemosphere*, *347*, 140578.

2. Asgari, E., Esrafili, A., Jafari, A. J., Kalantary, R. R., Nourmoradi, H., Farzadkia, M. (2019). The comparison of ZnO/polyaniline nanocomposite under UV and visible radiations for decomposition of metronidazole: degradation rate, mechanism and mineralization. *Process Safety and Environmental Protection*, *128*, 65–76.

3. Azizi, A. (2020). Green synthesis of Fe_3O_4 nanoparticles and its application in preparation of Fe_3O_4/cellulose magnetic nanocomposite: a suitable proposal for drug delivery systems. *Journal of Inorganic and Organometallic Polymers and Materials*, *30*, 3552–3561.

4. Bala, N., Napiah, M., Kamaruddin, I. (2017). Application of response surface methodology for mix design optimization of nanocomposite modified asphalt mixtures. *GEOMATE Journal*, *13*(39), 237–244.

5. Bashiri, F., Khezri, S. M., Kalantary, R. R., Kakavandi, B. (2020). Enhanced photocatalytic degradation of metronidazole by TiO2 decorated on magnetic reduced graphene oxide: Characterization, optimization and reaction mechanism studies. *Journal of Molecular Liquids*, *314*, 113608.

6. Betiku, E., Osunleke, A. S., Odude, V. O., Bamimore, A., Oladipo, B., Okeleye, A. A., Ishola, N. B. (2021). Performance evaluation of adaptive neuro-fuzzy inference system, artificial neural network and response surface methodology in modeling biodiesel synthesis from palm kernel oil by transesterification. *Biofuels*, *12*(3), 339–354.

7. Cai, H., Zhao, T., Ma, Z., Liu, J. (2020). Efficient removal of metronidazole by the photo-Fenton process with a magnetic Fe3O4@ PBC composite. *Journal of Environmental Engineering*, *146*(7), 04020056.

8. Carrales-Alvarado, D. H., Rodríguez-Ramos, I., Leyva-Ramos, R., Mendoza-Mendoza, E., Villela-Martínez, D. E. (2020). Effect of surface area and physical–chemical properties of graphite and graphene-based materials on their adsorption capacity towards metronidazole and trimethoprim antibiotics in aqueous solution. *Chemical Engineering Journal*, *402*, 126155.

9. Davarnejad, R., Hassanvand, Z. R., Mansoori, S., Kennedy, J. F. (2022). Metronidazole elimination from wastewater through photo-Fenton process using green-synthesized alginate-based hydrogel coated bimetallic iron-copper nanocomposite beads

as a reusable heterogeneous catalyst. *Bioresource Technology Reports*, *18*, 101068.

10. DineshKumar, S., Purushothaman, S. (2016). Synthesis and characterization of polymer nanocomposites for biomedical applications-current perspectives and challenges. *International Journal of Research in Engineering and Science (IJRES)*, *4*(10), 2320–9356.

11. Eskandari, P., Amarloo, E., Zangeneh, H., Rezakazemi, M., Aminabhavi, T. M. (2023). Photocatalytic degradation of metronidazole and oxytetracycline by novel l-Arginine (C, N codoped)-TiO_2/g-C_3N_4: RSM optimization, photodegradation mechanism, biodegradability evaluation. *Chemosphere*, *337*, 139282.

12. Eapen, J. V., Thomas, S., Antony, S., George, P., Antony, J. (2024). A review of the effects of pharmaceutical pollutants on humans and aquatic ecosystem. *Exploration of Drug Science*, *2*(5), 484–507.

13. Farzadkia, M., Esrafili, A., Baghapour, M. A., Shahamat, Y. D., Okhovat, N. (2014). Degradation of metronidazole in aqueous solution by nano-ZnO/UV photocatalytic process. *Desalination and Water Treatment*, *52*(25–27), 4947–4952.

14. Fiszka Borzyszkowska, A., Sulowska, A., Zekker, I., Karczewski, J., Bester, K., Zielińska-Jurek, A. (2022). Environmentally friendly fabrication of high-efficient Fe-ZnO/citric acid-modified cellulose composite and the enhancement of photocatalytic activity in the presence of H_2O_2. *Catalysts*, *12*(11), 1370.

15. Gahrouei, A. E., Vakili, S., Zandifar, A., Pourebrahimi, S. (2024). From wastewater to clean water: Recent advances on the removal of metronidazole, ciprofloxacin, and sulfamethoxazole antibiotics from water through adsorption and advanced oxidation processes (AOPs). *Environmental Research*, 119029.

16. Grenni, P., Ancona, V., Caracciolo, A. B. (2018). Ecological effects of antibiotics on natural ecosystems: A review. *Microchemical Journal*, *136*, 25–39.

17. Guo, H., Li, Z., Xiang, L., Jiang, N., Zhang, Y., Wang, H., Li, J. (2021). Efficient removal of antibiotic thiamphenicol by pulsed discharge plasma coupled with complex catalysis using graphene-WO3-Fe_3O_4 nanocomposites. *Journal of Hazardous Materials*, *403*, 123673.

18. Ighalo, J. O., Igwegbe, C. A., Adeniyi, A. G., Adeyanju, C. A., Ogunniyi, S. (2020). Mitigation of Metronidazole (Flagyl) pollution in aqueous media by adsorption: a review. *Environmental Technology Reviews*, *9*(1), 137–148.

19. Kumar, A., Kumar, V., Singh, B. (2021). Cellulosic and hemicellulosic fractions of sugarcane bagasse: Potential, challenges and future perspective. *International Journal of Biological Macromolecules*, *169*, 564–582.

20. Lalegül-Ülker, Ö., Elçin, Y. M. (2021). Magnetic and electrically conductive silica-coated iron oxide/polyaniline nanocomposites for biomedical applications. *Materials Science and Engineering: C*, *119*, 111600.

21. Malika, M., Sonawane, S. S. (2021). Application of RSM and ANN for the prediction and optimization of thermal conductivity ratio of water based Fe_2O_3 coated SiC hybrid nanofluid. *International Communications in Heat and Mass Transfer*, *126*, 105354.

22. Mansoori, S., Davarnejad, R., Ozumchelouei, E. J., Ismail, A. F. (2021). Activated biochar supported iron-copper oxide bimetallic catalyst for degradation of ciprofloxacin via photo-assisted electro-Fenton process: a mild pH condition. *Journal of Water Process Engineering*, *39*, 101888.

23. Mehta, R. V., Upadhyay, R. V., Charles, S. W., Ramchand, C. N. (1997). Direct binding of protein to magnetic particles. *Biotechnology Techniques*, *11*, 493–496.

24. Mosavi, S. A., Ghadi, A., Gharbani, P., Mehrizad, A. (2021). Photocatalytic removal of methylene blue using Ag@ CdSe/zeoilte nanocomposite under visible light irradiation by response surface methodology. *Materials Chemistry and Physics*, *267*, 124696.

25. Mun, S., Yadav, M., Kim, J.-H., Kim, J. (2015). Synthesis and characterization of iron oxide-cellulose nanocomposite films.

26. Olatunji, O. (2016). Classification of natural polymers. *Natural polymers: industry techniques and applications*, 1–17.

27. Pastrana-Martínez, L. M., Pereira, N., Lima, R., Faria, J. L., Gomes, H. T., Silva, A. M. T. (2015). Degradation of diphenhydramine by photo-Fenton using magnetically recoverable iron oxide nanoparticles as catalyst. *Chemical Engineering Journal*, *261*, 45–52.

28. Rajabi, S., Nasiri, A. (2021). Metronidazole photodegradation by a new nano-biomagnetic photocatalyst $ZnFe_2O_4$@ Methylcellulosee.

29. Rehm, B. H. A. (2010). Bacterial polymers: biosynthesis, modifications and applications. *Nature Reviews Microbiology*, *8*(8), 578–592.

30. Santana, D. R., Espino-Estévez, M. R., Santiago, D. E., Méndez, J. A. O., González-Díaz, O., Doña-Rodríguez, J. M. (2017). Treatment of aquaculture wastewater contaminated with metronidazole by advanced oxidation techniques. *Environmental nanotechnology, monitoring & management*, *8*, 11–24.

31. Sun, Y., Yang, Z., Tian, P., Sheng, Y., Xu, J., Han, Y.-F. (2019). Oxidative degradation of nitrobenzene by a Fenton-like reaction with Fe-Cu bimetallic catalysts. *Applied Catalysis B: Environmental*, *244*, 1–10.

32. Titouhi, H., Belgaied, J.-E. (2016). Removal of ofloxacin antibiotic using heterogeneous Fenton process over modified alginate beads. *Journal of Environmental Sciences*, *45*, 84–93.

33. Wang, J., Liu, C., Qi, J., Li, J., Sun, X., Shen, J.,… Wang, L. (2018). Enhanced heterogeneous Fenton-like systems based on highly dispersed Fe0-Fe2O3 nanoparticles embedded ordered mesoporous carbon composite catalyst. *Environmental Pollution*, *243*, 1068–1077.

34. Wang, P., Wu, D., You, X., Su, Y., Xie, B. (2021). Antibiotic and metal resistance genes are closely linked with nitrogen-processing functions in municipal solid waste landfills. *Journal of Hazardous Materials*, *403*, 123689.

35. Wang, S., Lu, A., Zhang, L. (2016). Recent advances in regenerated cellulose materials. *Progress in Polymer Science*, *53*, 169–206.

36. Wang, X., Zhang, X., Zhang, Y., Wang, Y., Sun, S.-P., Wu, W. D., Wu, Z. (2020). Nanostructured semiconductor supported iron catalysts for heterogeneous photo-Fenton oxidation: a review. *Journal of Materials Chemistry A*, *8*(31), 15513–15546.

37. Xiong, R., Wang, Y., Zhang, X., Lu, C. (2014). Facile synthesis of magnetic nanocomposites of cellulose@ ultrasmall iron oxide nanoparticles for water treatment. *RSC Advances*, *4*(43), 22632–22641.

38. Yadav, M., Mun, S., Hyun, J., Kim, J. (2015). Synthesis and characterization of iron oxide/cellulose nanocomposite film. *International Journal of Biological Macromolecules*, *74*, 142–149.

39. Zaidi, N., Mir, M. A., Chang, S. K., Abdelli, N., Hasnain, S. M., Ali Khan, M. A., Andrews, K. (2025). Pharmaceuticals and personal care products as emerging contaminants: environmental fate, detection, and mitigation strategies. *International Journal of Environmental Analytical Chemistry*, 1–29.

40. Zhang, Y., Zuo, S., Zheng, Q., Yu, G., Wang, Y. (2024). Removal of antibiotic resistant bacteria and antibiotic resistance genes by an electrochemically driven UV/chlorine process for decentralized water treatment. *Water Research*, *265*, 122298.

41. Zhou, X., Liu, D., Zhang, Y., Chen, J., Chu, H., Qian, Y. (2018). Degradation mechanism and kinetic modeling for UV/peroxydisulfate treatment of penicillin antibiotics. *Chemical Engineering Journal*, *341*, 93–101.